Structure of Tropinone Reductase-II Complexed with NADP$^+$ and Pseudotropine at 1.9 Å Resolution: Implication for Stereospecific Substrate Binding and Catalysis‡

Atsuko Yamashita,[§,||] Hiroaki Kato,[*,§] Soichi Wakatsuki,[⊥] Takashi Tomizaki,[⊥] Toru Nakatsu,[§] Keiji Nakajima,[#] Takashi Hashimoto,[#] Yasuyuki Yamada,[#] and Jun'ichi Oda[*,§,△]

Institute for Chemical Research, Kyoto University, Uji, Kyoto 611-0011, Japan, ESRF, BP-220, Grenoble Cedex, France, and Graduate School of Biological Sciences, Nara Institute of Science and Technology, 8916-5 Takayama, Ikoma, Nara 630-0101, Japan

Received October 20, 1998; Revised Manuscript Received February 1, 1999

ABSTRACT: Tropinone reductase-II (TR-II) catalyzes the NADPH-dependent reduction of the carbonyl group of tropinone to a β-hydroxyl group. The crystal structure of TR-II complexed with NADP$^+$ and pseudotropine (ψ-tropine) has been determined at 1.9 Å resolution. A seven-residue peptide near the active site, disordered in the unliganded structure, is fixed in the ternary complex by participation of the cofactor and substrate binding. The ψ-tropine molecule is bound in an orientation which satisfies the product configuration and the stereochemical arrangement toward the cofactor. The substrate binding site displays a complementarity to the bound substrate (ψ-tropine) in its correct orientation. In addition, electrostatic interactions between the substrate and Glu156 seem to specify the binding position and orientation of the substrate. A comparison between the active sites in TR-II and TR-I shows that they provide different van der Waals surfaces and electrostatic features. These differences likely contribute to the correct binding mode of the substrates, which are in opposite orientations in TR-II and TR-I, and to different reaction stereospecificities. The active site structure in the TR-II ternary complex also suggests that the arrangement of the substrate, cofactor, and catalytic residues is stereoelectronically favorable for the reaction.

Tropinone reductase-II (TR-II, EC 1.1.1.236) is a key enzyme in the biosynthetic pathway of tropane alkaloids which include medicinally important compounds such as hyoscyamine (atropine) and cocaine. TR-II catalyzes an NADPH-dependent reduction of the 3-carbonyl group of tropinone to a β-hydroxyl group and produces pseudotropine (ψ-tropine; Scheme 1). The enzyme from *Datura stramonium* is a dimer of identical 28 kDa subunits (*1*). The deduced sequence of TR-II indicates that this enzyme is a member of the short-chain dehydrogenase/reductase (SDR)[1] family. Members of this family have a highly conserved Tyr-X-X-X-Lys sequence which is thought to be essential for their catalytic activities (*2*).

There is another tropinone reductase in the metabolic pathway, tropinone reductase-I (TR-I, EC 1.1.1.206). TR-I reduces the same substrate tropinone but produces tropine with an α-hydroxyl group, which has a different diastereomeric configuration from the product of TR-II (Scheme 1).

Scheme 1

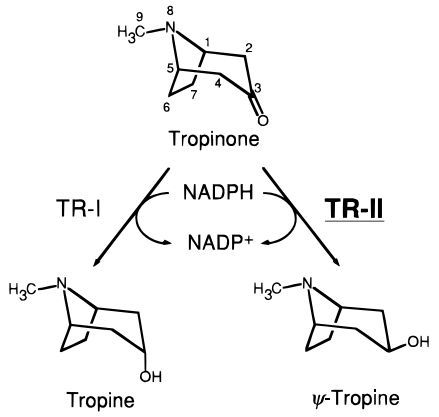

Despite this difference of reaction stereospecificity, TR-II and TR-I share 64% identical amino acid residues (*3*), have similar K_m values for NADPH, and catalyze the *pro-S* hydride transfer to tropinone (*4*). Therefore, it is of interest to elucidate the structural basis for the reaction stereospecificity and substrate specificity of both TRs.

Crystallographic analysis of TR-II and TR-I has revealed a striking resemblance of the overall folds of the two enzymes (*5*). The architectures of NADP(H) binding sites in both TRs are also similar, suggesting similar binding modes of NADP(H) in TR-II and TR-I. The tropinone binding mode was modeled from the unliganded TR structures; TR-II and TR-I presumably bind their substrates in different orientations toward the *pro-S* hydride of NADPH

‡ The coordinates have been deposited with the Brookhaven Protein Data Bank for immediate release (accession code 2ae2).

* To whom correspondence should be addressed.
§ Kyoto University.
|| Present address: RIKEN Harima Institute, 323-3, Mihara, Mikazuki, Hyogo 679-5143, Japan.
⊥ ESRF.
Nara Institute of Science and Technology.
△ Present address: Fukui Prefectural University, 4-1-1 Kenjojima, Matsuoka, Fukui 910-1195, Japan.

[1] Abbreviations: rmsd, root-mean-square difference; SDR, short-chain dehydrogenase/reductase; TR, tropinone reductase; ψ-tropine, pseudotropine.

10.1021/bi9825044 CCC: $18.00
Published on Web 05/26/1999

in order to catalyze the production of different tropine isomers. Further crystal structure analysis is needed to prove this presumption and to reveal the detailed architecture required for substrate binding.

The NADPH-dependent oxidoreduction of TRs is likely to proceed by a sequential bi−bi mechanism with the enzyme binding the substrate and cofactor simultaneously. To elucidate the important intermolecular interactions relevant to the catalytic mechanism, it is necessary to analyze structures of TRs complexed with both the substrate and the cofactor at high resolution. There are four possible combinations of a cofactor and a substrate for making a ternary complex of TR: in the TR-II case, (a) NADPH and tropinone (the forward reaction complex), (b) $NADP^+$ and ψ-tropine (the reverse reaction complex), (c) $NADP^+$ and tropinone (a nonproductive complex), and (d) NADPH and ψ-tropine (another nonproductive complex). It has been reported that the rate of the reverse reaction of TR-II is much slower than that of the forward reaction (*4*). Thus it is expected to make a stable productive complex of TR-II with $NADP^+$ and ψ-tropine (combination b).

In this study, we have determined the structure of TR-II from *D. stramonium* complexed with $NADP^+$ and ψ-tropine at 1.9 Å resolution. This structure reveals the substrate and cofactor binding mode in the enzyme. The structure also indicates that ligand binding orders a peptide in the active site that is unobservable in the apoenzyme (*5*). The active site structure provides an insight into the architecture of the TR-II active site for its stereospecific oxidoreduction.

MATERIALS AND METHODS

Crystallization. TR-II from *D. stramonium* was expressed in *Escherichia coli* and purified as previously described (*6*). ψ-tropine was synthesized and purified according to the published procedure (*7*).

Crystals of the TR-II ternary complex were obtained by cocrystallization with the ligands using the hanging-drop vapor diffusion method. Two microliters of the protein solution (15 mg/mL TR-II, 4 mM $NADP^+$, 20 mM ψ-tropine, 5 mM Tris-HCl, pH 7.5, and 1 mM DTT) was mixed with 2 μL of the reservoir solution (0.1 M HEPES, pH 7.5, 1.7 M Li_2SO_4, and 1 mM DTT) to form a hanging drop, and the drop was equilibrated over 1 mL of the reservoir solution at 20 °C. K_m values for the substrates and cofactors of TR-II have been reported as several tens to hundreds micromolar range under a physiological condition (*4*). Single crystals (approximately 0.8 × 0.4 × 0.4 mm) were harvested after 2 weeks. These crystals have a space group of $P6_122$ or $P6_522$ and unit cell dimensions of $a = b = 88.6$ Å and $c = 338.3$ Å (Table 1).

X-ray Data Collection and Processing. X-ray diffraction data of the TR-II complex crystals were collected on the ID14/EH3 beamline at the European Synchrotron Radiation Facility (ESRF, Grenoble, France) at room temperature with a wavelength of 0.918 Å using a 40 × 80 cm Fuji imaging plate detector. The crystal to film distance was 360 mm and the detector 2θ angle was 0°. The oscillation range was 3°, and the exposure time was 60 s (two passes of 30 s exposure). The data up to 1.9 Å resolution were processed with DENZO and SCALEPACK (*8*). The final data set was put on a quasi-absolute scale using TRUNCATE of the CCP4 package (*9*).

Table 1: Statistics of Data Collection and Structure Refinement

(1) Data Collection	
space group	$P6_122$
cell dimensions (Å)	$a = b = 88.6$
	$c = 338.3$
subunit/asymmetric unit	2
V_m (Å^3/Da)	3.39
V_{solv} (%)	63.7
resolution (Å)	1.9
observed reflections	195899
unique reflections	54120
completeness (%) (overall/last shell)	85.6/77.9 (1.93−1.90 Å)
R_{merge}[a] (%) (overall/last shell)	8.4/24.7
(2) Refinement	
resolution (Å)	10.0−1.90
protein atoms	3950
ligand atoms	116
water molecules	236
R-factor[b]/R_{free} (%)	17.2/20.6
rms deviations	
bond length (Å)	0.007
bond angles (deg)	1.275
dihedral angles (deg)	23.836
improper angles (deg)	0.806
average B (Å^2)	
main chain	16.0
side chain	20.7
solvent	32.3

[a] $R_{merge} = |I - \langle I \rangle|/I$. [b] R-factor $= ||F_o| - |F_c||/|F_o|$ (5% randomly omitted reflections were used for R_{free}).

Data collection and processing statistics are presented in Table 1.

Structure Determination. The structure of the TR-II complex was solved by molecular replacement with AMORE (*10*), using the coordinates of the TR-II apoenzyme determined with the multiple isomorphous replacement method (*5*) (PDB entry 2ae1) as a search model. A single subunit was used. A cross-rotation function, calculated from the data in a 10−3.5 Å resolution range, showed two prominent peaks with heights of 9.1σ and 6.9σ. During the translational search, both enantiomeric space groups $P6_122$ and $P6_522$ were tried, and clear solutions for both rotation functions mentioned above were detected in space group $P6_122$. One of the solutions was fixed, and the search for the other translational solution was repeated. The model was refined as two rigid bodies using AMORE with a correlation coefficient of 0.734 and an R-factor of 31.9% for the range of 10−3.5 Å. Electron densities for the bound $NADP^+$, ψ-tropine, and residues from 195 to 201, which were not included in the search model coordinates, were clearly defined at this stage. The model of the residues from 195 to 201 was built with TURBO−FRODO (*11*). Refinement was carried out using X-PLOR 3.851 (*12*). In subsequent positional refinement and group B-factor refinement, $NADP^+$ and ψ-tropine models were included to fit the Fourier maps. The coordinates, parameter file, and topology file for ψ-tropine were generated using QUANTA and CHARMm (Molecular Simulations Inc.). The model was then subjected to several cycles of positional refinement, individual B-factor refinement, and rebuilding against data in the resolution range of 10−1.9 Å. Water molecules were included using WATERHUNTER (*13*). The geometry of the model was monitored throughout the refinement using X-PLOR and PROCHECK (*14*). Statistics on the refinement and the model geometry are presented in Table 1.

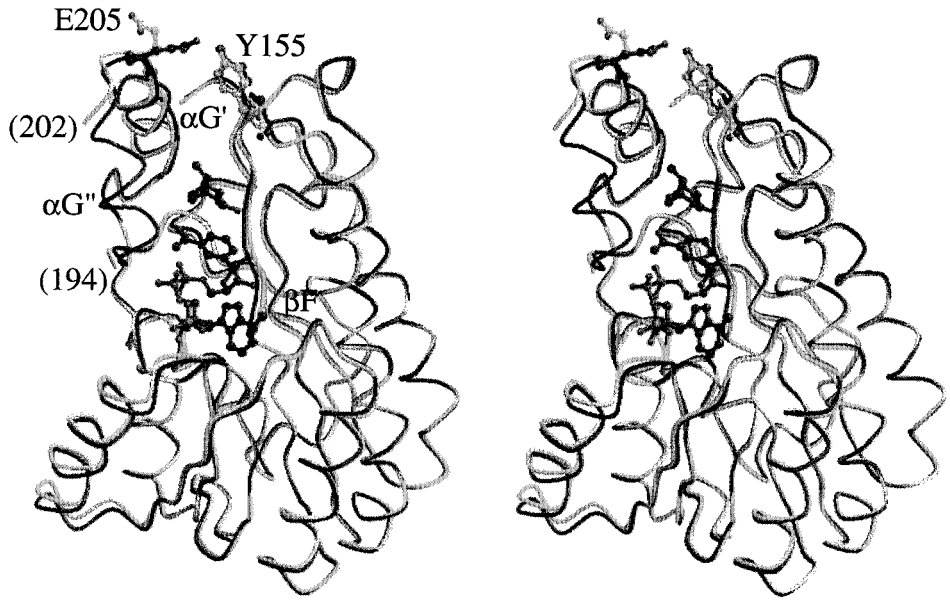

FIGURE 1: Superposition of the subunit structures of the unliganded TR-II and TR-II−$NADP^+$−ψ-tropine complex. Coordinates were superimposed using the program LSQKAB (*9*). The Cα backbones of the unliganded TR-II and the ternary complex are shown in light gray and dark gray, respectively. The positions of residues 194 and 202 are shown. Tyr155, Glu205, bound $NADP^+$, and ψ-tropine are illustrated in ball-and-stick models. The figure was generated by MOLSCRIPT (*31*).

Measurement of the NADPH Content in Reaction Mixtures. The amount of NADPH in reaction mixtures of TR-II was measured spectrophotometrically. Reaction mixtures A (0.1 M HEPES, pH 7.5, 1.7 M Li_2SO_4, 1 mM DTT, 4 mM $NADP^+$, 20 mM ψ-tropine, and 1.0 or 5.0 μM TR-II) and B (0.1 M HEPES, pH 7.5, 1.7 M Li_2SO_4, 1 mM DTT, 4 mM NADPH, 20 mM tropinone, and 1.0 or 5.0 μM TR-II) were allowed to reach an equilibrium state at 20 °C for several days. The NADPH concentration of each solution was calculated from the absorbance at 340 nm using a molar absorption coefficient of 6200 M^{-1} cm^{-1}.

RESULTS AND DISCUSSION

Ternary Complex of TR-II. The ternary complex including TR-II, $NADP^+$, and ψ-tropine was crystallized under a completely different condition from that of the unliganded TR-II, and it gave crystals with different space group and cell parameters. Although the unit cell dimensions were large and the solvent content was rather high (Table 1), the crystals diffracted well to a high resolution, 1.5 Å, on the third station of beamline ID14 at the ESRF. The diffraction data up to 1.9 Å resolution had sufficient accuracy and allowed an analysis of the structure. The final model of the TR-II−$NADP^+$−ψ-tropine complex was a dimer including all residues except for the first N-terminal residue, which was found to be cleaved after purification from *E. coli* (data not shown). The model was refined to an *R*-factor of 17.2% and R_{free} of 20.6% for the reflections between 10.0 and 1.9 Å resolution. The model has 91% of the residues in the most favored Ramachandran regions with no residue in the disallowed regions.

The ligands of the TR-II ternary complex were assumed to be in a certain equilibrium state between substrates ($NADP^+$ and ψ-tropine) and products (NADPH and tropinone) of the reverse reaction. Since TR-II has catalytic activity even in the crystalline state (data not shown), the elucidated structure of the TR-II complex (and therefore its ligands) is considered to reflect that of TR-II in solution at the equilibrium state. Thus, we estimate the ratio of the substrates to the products in the crystal from that of reaction mixtures. TR-II in solution was allowed to react to reach the equilibrium in two different conditions: one which is similar to the crystallization condition (the reverse reaction condition) and another which is similar but containing NADPH and tropinone instead of $NADP^+$ and ψ-tropine (the forward reaction condition). Then NADPH contents in these solutions were measured. Both solutions of the reverse and forward reaction conditions reached an equilibrium about 4 days after the reaction began, and they exhibited a similar $NADP^+$/NADPH ratio; the proportions of NADPH to the total dinucleotide contents in both the reverse and forward reaction conditions were 4.1% after 10 days of incubation.[2] The results suggest that more than 95% of the TR-II molecule in the crystal existed as a complex with $NADP^+$ and ψ-tropine. Thus $NADP^+$ and ψ-tropine models rather than NADPH and tropinone models were used in the refinement process and further discussion.

Description of the Structure. The TR-II dimer is very symmetrical and the Cα coordinates of the two subunits (hereafter referred to as subunits A and B) are superimposed with a root-mean-square deviation (rmsd) of 0.14 Å. Therefore, the structure of subunit A is considered representative of the two subunits hereafter. The subunit structure of the ternary complex is shown in Figure 1; it is an α/β doubly wound protein with a Rossmann fold for NADPH binding. Overall, the structure of the ternary complex is similar to that of the unliganded TR-II (*6*) and has essentially the same secondary structure assignments. A superposition of the subunits of the ternary complex and the unliganded

[2] The NADPH content plateaued between 4 and 10 days, and after 10 days of incubation, the NADPH content proceeded to decrease due to its decomposition.

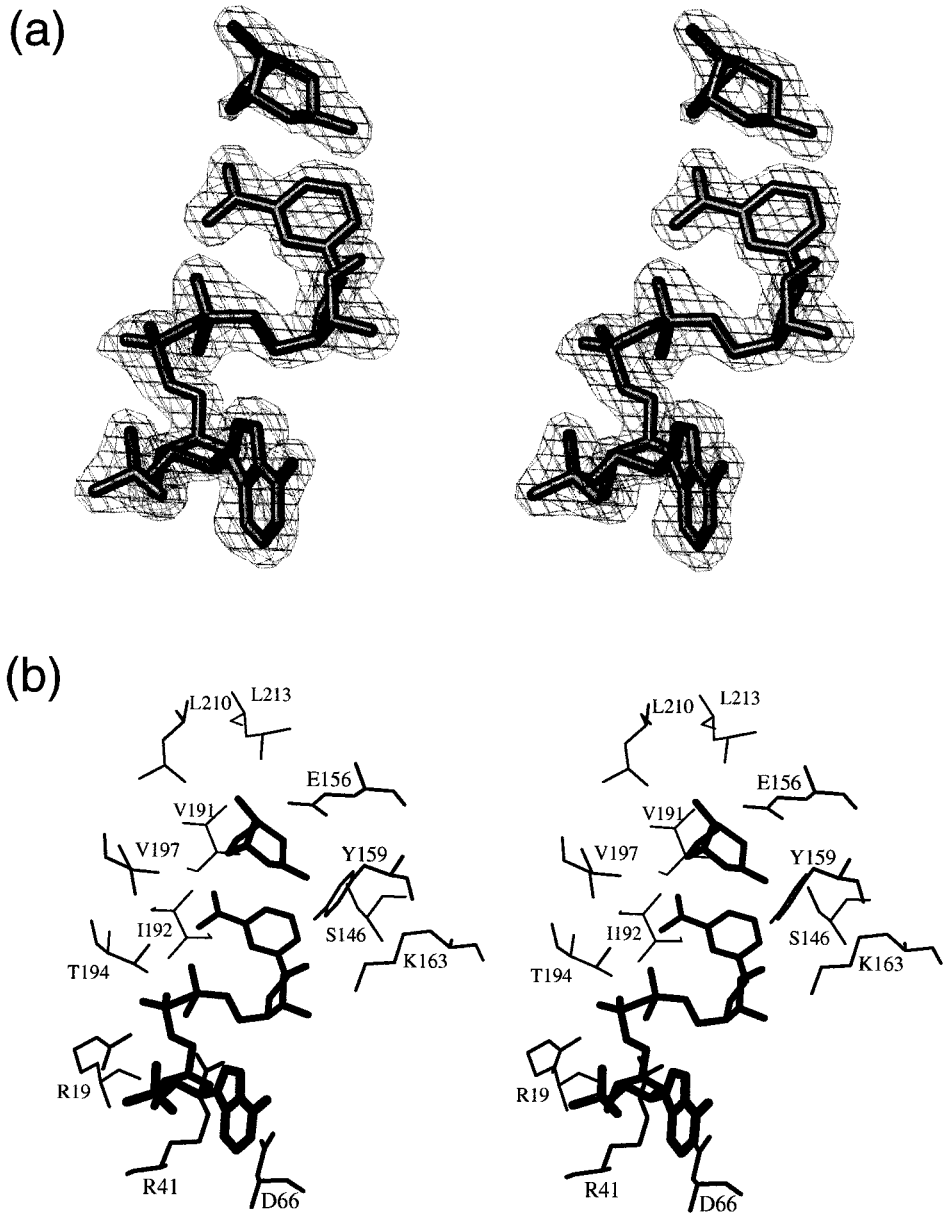

FIGURE 2: (a) Stereoview of the electron density map at 1.9 Å resolution for the ligands, $NADP^+$, and ψ-tropine at the active site in subunit A. The $F_o - F_c$ omit map, contoured at the 3.5σ level, was calculated with the refined model excluding the ligands. The figure was produced with TURBO−FRODO (*11*). (b) Stereoview of the ψ-tropine and $NADP^+$ binding sites. ψ-tropine (above) and $NADP^+$ (below) are illustrated in thick lines. The figure was generated by MOLSCRIPT (*31*).

structure using 252 out of the 259 residues showed an rmsd between Cα atoms of only 0.41 Å (Figure 1).

This ternary complex further revealed the structure of the protein backbone and side chains between residues 195 and 201. These residues, which are disordered and not modeled in the unliganded TR-II structure, were clearly visible in the electron density map of the complex and were modeled as an α-helical structure. The corresponding peptide in the TR-I structure is also a helix, αG″ (*5*). Thus we define this segment as αG″. This helix is connected to βF (N-terminal side) and αG′ (C-terminal side) with two loop regions, Gly190−Thr194 and Ile201−Asp203, respectively. The length of αG″ is three residues shorter than TR-I, and the C-terminal side loop is longer instead.

$NADP^+$ Binding Site. The electron density corresponding to $NADP^+$ and ψ-tropine was very well defined (Figure 2a). A close-up view of their binding sites is shown in Figure 2b. The $NADP^+$ molecules bind at the bottom of the cleft between the small lobe (αG″ and αG′) and the core domain (the remaining main part with the Rossmann fold, defined in ref *5*). The $NADP^+$ is found in an extended conformation. The nicotinamide ring is in the *syn* conformation and has its B face oriented toward the ψ-tropine, consistent with a *pro-S* hydride transfer. Both ribose rings have the C2′-*endo* puckering.

Figure 3 shows the environment of the $NADP^+$ binding site. The nicotinamide ring and pyrophosphate moiety make polar interactions with the main chain of Ile192 and the side chains of Thr194 and Ser195. These residues are located in the N-terminal side loop or the N-terminal part of αG″. These interactions are likely to be responsible for holding the loop structure, and therefore the position of αG″ is fixed in the complex. In addition, Glu205, which is the N-terminal residue of αG′ and interacts with an adjacent subunit in the

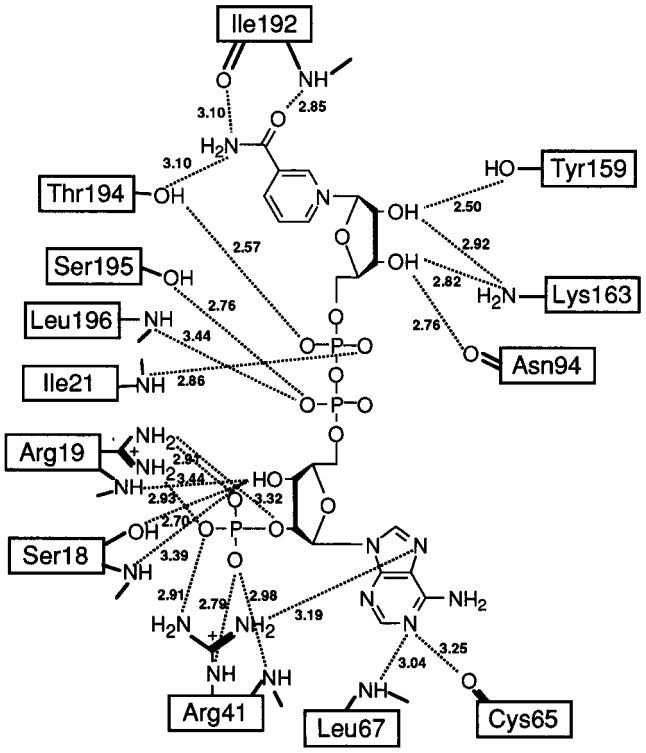

FIGURE 3: Schematic view of the interactions of $NADP^+$ with TR-II. Possible hydrogen bonds are indicated with dashed lines. The distances (observed in subunit A, ≤3.4 Å) are in angstroms.

unliganded crystal, makes a hydrogen bond with Tyr155 located in the core domain of the same subunit in this structure (Figure 1). We suggest that this interaction acts as a lock for the proper positioning of αG″ in the complex. These results indicate that αG″, which is located near the TR-II active site, is disordered while the substrate and the cofactor do not bind at the active site and becomes fixed and completes the active site when the cofactor binds. This fixed αG″ is also considered to provide necessary complementarity to the bound substrate, which is important for the substrate recognition (described below).

The 2′-phosphate group of the adenine ribose of $NADP^+$ makes electrostatic and hydrogen-bonding interactions with Arg19 and Arg41. The side chain conformations of these residues are changed from those found in the unliganded TR-II. The side chain of Arg19 interacts with Thr194 in the unliganded structure, in which αG″ is disordered and is not positioned properly for catalysis. In the ternary complex, however, the side chain of Arg19 flips toward the 2′-phosphate group. Consequently, the Cα position of Thr194 moved by 1.18 Å toward the active site from the position in the unliganded structure. Removing the interaction of Arg19 with Thr194 may also be necessary to allow αG″ to take the proper geometry for catalysis. The side chain of Arg41 also tilts toward the 2′-phosphate group. The distances between the guanidino group of Arg41 and the phosphate group of $NADP^+$ are about 2.8 Å (Figure 3).

Other interactions with $NADP^+$ present in this structure are similar to those in the TR-I structure complexed with $NADP^+$ (*5*) or structures of other SDR enzymes complexed with cofactor or with both cofactor and substrate (*15*−*22*).

ψ-Tropine Binding Site. The ψ-tropine molecules were found in the cleft between the small lobe and the core domain, directly above the B face of nicotinamide ring of $NADP^+$ molecules. The electron density map showed the piperidine ring to be in the chair form with the CH_3 group on the nitrogen atom in equatorial position with respect to this ring. The conformation of ψ-tropine in the binding site was the same as that of the structure of free ψ-tropine, which was determined independently with X-ray crystallography (*23*).

The binding site shows a high degree of complementarity to the substrate (Figure 4a). The total buried surface for ψ-tropine is 299 $Å^2$, which is 98% of the surface area for free ψ-tropine. The binding site has a pocket which complements the C6−C7 methylene bridge of the substrate at the corresponding position. If the substrate were bound to the active site in the opposite orientation, steric clashes between the methylene bridge and residues in the binding site, such as Glu156, would occur. The van der Waals contacts between a substrate (ψ-tropine or tropinone) and TR-II likely contribute to proper substrate orientation.

The binding site is mainly surrounded by hydrophobic residues (Val147, Val191, Leu196, Val197, Leu210, Leu213), most of which are located in helices αG″ (195−201) and αG′ (204−210) (Figure 4b). Since these residues are positioned near the nonpolar part of ψ-tropine, such as the methyl group and the methylene bridge, a significant part of the binding energy is likely to be derived from these hydrophobic interactions. Furthermore, Glu156 is located near the amine moiety of the substrate (the distance between the carboxyl group of Glu156 and the amine moiety of the substrate is about 2.8 Å). The electrostatic interaction between the positive charge of the amine moiety of the substrate and negative charge of Glu156 is likely to fix the position of the substrate, which is orienting its α side (the opposite side of the seven-membered ring from the methylamine side) toward the *pro-S* hydride of NADPH. This binding orientation of the substrate is essential to produce the β-hydroxyl group in tropinone reduction of TR-II. The ψ-tropine binding mode observed in this structure is in accordance with the assumption from the unliganded structure (*5*).

This TR-II ternary complex also enables us to discuss differences of the active site structures between TR-II and TR-I. In TR-I, the substrate is assumed to bind in the "upside-down" orientation relative to the substrate in TR-II in order to form a product (tropine) with a configuration different from that of the TR-II product (ψ-tropine) (*5*). Figure 4c shows the active site in TR-I with tropinone binding in the predicted orientation. The TR-I active site also shows complementarity to the substrate. If tropinone were bound to TR-I in the opposite orientation, it would not fit well in the binding site and it might be difficult to maintain the correct geometry for the reaction. As shown in Figure 4, the tropinone binding site in TR-I has a different shape compared to that of TR-II, and this difference arises from different kinds of residues at the corresponding positions such as Leu165 (TR-I) and Val153 (TR-II), Ile223 (TR-I) and Leu210 (TR-II), and Phe226 (TR-I) and Leu213 (TR-II). These results indicate that TR-II and TR-I exhibit several different amino acid residues in their active sites to provide complementarity to the substrate structures in their different correct binding orientations. The substrate orientations in TRs are further supported by the electrostatic interactions. Glu156 in TR-II, which plays a key role to fix the substrate with an

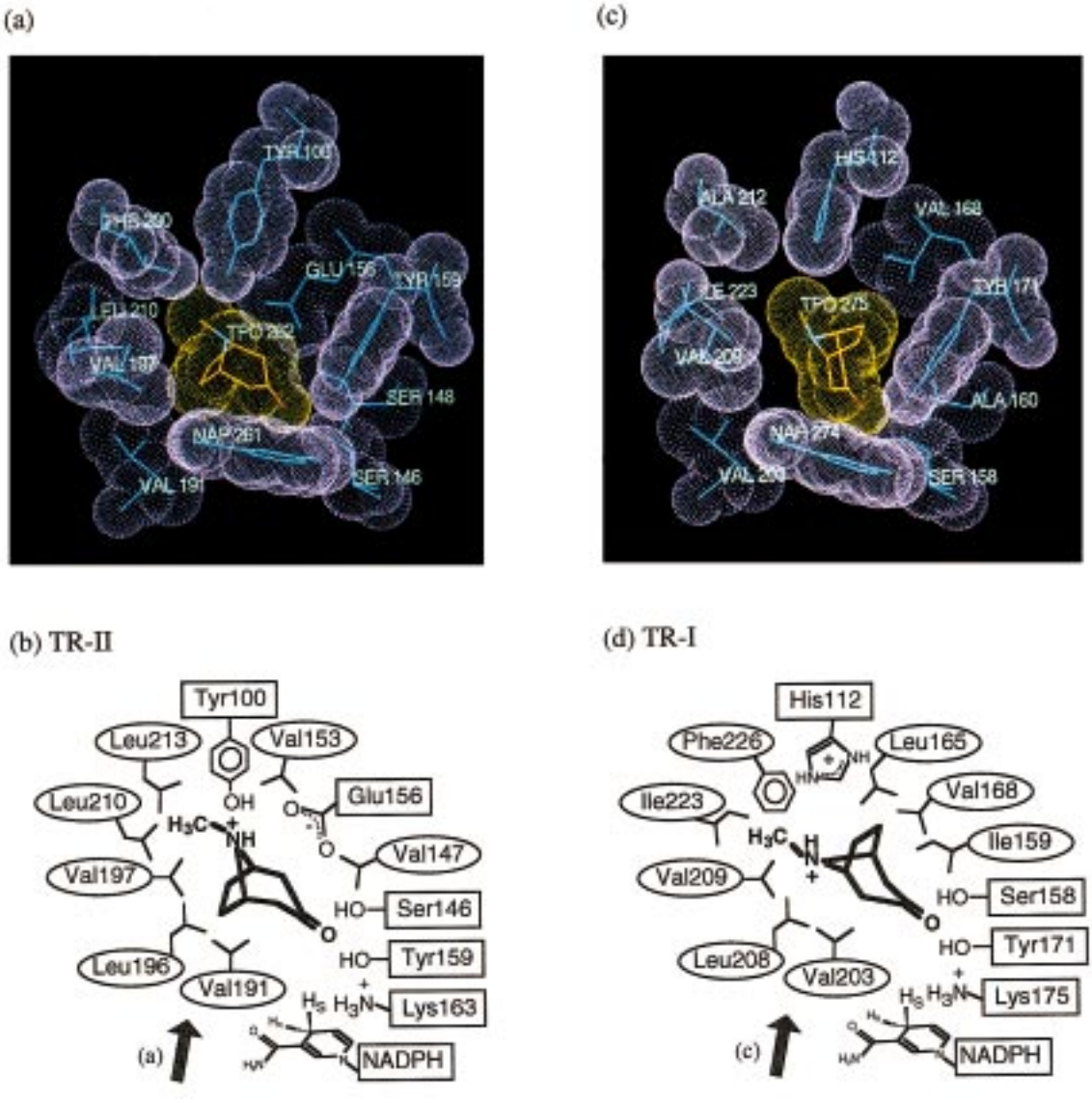

FIGURE 4: Importance of complementarity between the substrate and the active sites of TR-II and TR-I for stereospecific recognition. The model of tropinone, the common substrate for the forward reaction of both TRs, is predicted and shown as the bound substrate in order to compare the binding sites of TR-II and TR-I. (a) Dotted van der Waals surfaces of the active site cavity in TR-II. The tropinone model is built using the tropane ring of bound ψ-tropine in the TR-II ternary complex. Surfaces of the active sites are shown in purple and those of tropinone in yellow. Abbreviations: NAP, $NADP^+$; TPO, tropinone. (b) Schematic view of the active site in TR-II. Tropinone is illustrated in thick lines. The arrow indicates the viewing direction of panel a. (c) Dotted van der Waals surfaces of the active site cavity in TR-I. The model of the tropinone molecule bound in TR-I was constructed as follows: the tropinone model of TR-II shown in panel a was turned over, and the plane of its carbonyl group is superimposed with the original one so as to maintain the geometry of the plane of the carbonyl group toward the *pro-S* hydride of NADPH and the catalytic tyrosine residue, Tyr171. Other settings are the same as in panel a. (d) Schematic view of the active site in TR-I. The arrow indicates the viewing direction of panel c. Panels a and c were generated with TURBO−FRODO (*11*).

electrostatic interaction, is replaced by Val168 in TR-I, and Tyr100 in TR-II is replaced by His112 in TR-I. Even if the substrate in TR-I binds with the same orientation as in TR-II, the positive charge of His112 may cause charge repulsion with the substrate. The binding orientation of the substrate in TR-I is therefore fixed to the opposite of that in TR-II. In addition, the difference of electrostatic interactions in TR-II and TR-I might be responsible for the length of αG″. TR-I has about one turn (three residues) longer αG″ than TR-II, and the C-terminal residues in αG″ interact with the N-terminal residues in αG′. This interaction is likely to hold the position of αG″ and to make the binding site more rigid. Thus the active site in TR-I might provide proper binding of the substrate and compensate for the disadvantage of weaker electrostatic interaction (charge repulsion). In other words, TR-II has stronger electrostatic interaction (charge attraction); therefore, it adopts a loop structure, which is more flexible and facilitates the turnover.

Enzymes of the SDR family including TR-I and TR-II contain a highly conserved Ser-Tyr-Lys triad at the active site, and mechanistic proposals have focused on the central role of these residues in catalysis (*15*−*18*, *20*, *22*, *24*, *25*). These conserved residues are in fact located around the hydroxyl group of ψ-tropine in the ternary complex of TR-II (Figures 2b and 4b). The distance between the hydroxyl group of ψ-tropine and Tyr159 Oη (2.71 Å) suggests that

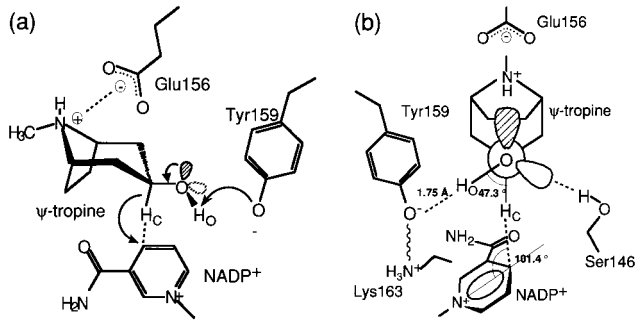

FIGURE 5: Scheme of the proposed mechanism of ψ-tropine oxidation. (a) The reaction implies the transfer of the ψ-tropine O3 proton (H_O) to Tyr159 Oη and the nucleophilic attack of the ψ-tropine C3 hydride (H_C) on the nicotinamide C4 of $NADP^+$. The description in terms of the sp^3-hybridized lone pair is used as the nonbonding electron pairs of oxygen. (b) Orthogonal view of (a) along the O3−C3 bond of ψ-tropine. The spatial organization of TR-II catalytic residues, $NADP^+$, ψ-tropine, and the orbitals of lone pair electrons on the oxygen are illustrated.

Tyr159 should be able to act as a general acid/base catalyst in the TR-II active site. Ser146 is within hydrogen-bonding distance to the hydroxyl group of ψ-tropine from the opposite direction of Tyr159. The distance between Lys163 Nη and Tyr159 Oη is 4.32 Å, and Lys163 could reduce the pK_a of Tyr159 by electrostatic interaction. In addition, Lys163 is also responsible for $NADP^+$ binding (Figure 3b). These observations are in agreement with the mechanism proposed in other SDR enzymes. The three catalytic residues are also structurally conserved in TR-I (*5*).

Active Site Architecture and Implication for Catalysis. This TR-II ternary complex structure also sheds light on the catalytic mechanism for the oxidation of ψ-tropine to tropinone, as the spatial organization of all participants is now completely defined. The reaction implies the proton transfer to Tyr159 Oη from the hydroxyl group of ψ-tropine and the nucleophilic attack of the hydride at C3 on C4 of the nicotinamide ring of $NADP^+$ (Figure 5a). Since hydrogen positions cannot be seen in electron density maps, we made models of hydrogen atoms on O3 or on C3, defined as H_O and H_C, respectively, using QUANTA (Molecular Simulations Inc.) with the theoretical O−H or C−H bond length. The position of the H_C atom could be modeled unequivocally with the tetrahedral coordination of the carbon atom. Though the C3−O3 bond can rotate freely, the H_O atom was assumed to be at the closest position to Tyr159 Oη, since the proton transfer is likely to occur under these conditions. The hydrogen placed in this way was 1.75 Å apart from Tyr159 Oη in subunit A.

The dihedral angle between C4−C3−O3−H_O is observed as 47.3°. In this geometry, the orbital of the lone pair of electrons on O3 is likely to be near *anti*-periplanar to H_C, which is an energetically favorable conformation for elimination of H_C, proposed as stereoelectronic effects (*26*, *27*) (Figure 5b). In the ternary complex, the side chain of Tyr159 changed its conformation slightly from the unliganded structure (the difference of the χ_1 angle is −6.0°) and seems to take this favorable position because of the interactions with ψ-tropine O3 and $NADP^+$ O2′N. Furthermore, the angle between N−C4−H_C is observed as 101.4° (Figure 5b). Attack angles in model hydride transfer reactions and in dehydrogenase reactions have been calculated by various computational methods, and in most cases this angle was calculated as obtuse angles between 102° and 119° (*28*−*30*). Thus the N−C4−H_C angle seen in the TR-II ternary complex is appropriate for the hydride attack on the $NADP^+$ nicotinamide ring. The reaction pathway for the reverse of the reaction is the exact opposite of the pathway for the forward direction. These results suggest that the arrangement of the substrate, the cofactor, and the catalytic residues is stereoelectronically favorable for the reaction proceeding.

The structure of TR-II complexed with $NADP^+$ and ψ-tropine revealed the active site architecture of this enzyme and the structure of the bound substrates. The part of the active site in TR-II, αG″, that is flexible in the unliganded enzyme is observed as ordered structure in the ternary complex. Therefore, the active site seems to be arranged properly for the catalytic reaction only after the substrates bind. The active site architecture also provides the complementarity between the active site and substrates to maintain its stereospecificity and to make the catalytic reaction favorable.

ACKNOWLEDGMENT

We thank Dr. B. L. Stoddard (Fred Hutchinson Cancer Research Center) for critical reading of the manuscript.

SUPPORTING INFORMATION AVAILABLE

A detailed description of X-ray data collection and processing with 1 figure and 1 table. This material is available free of charge via the Internet at http://pubs.acs.org.

REFERENCES

1. Nakajima, K., Hashimoto, T., and Yamada, Y. (1993) *Proc. Natl. Acad. Sci. U.S.A. 90*, 9591−9595.
2. Jörnvall, H., Persson, B., Krook, M., Atrian, S., Gonzàlez-Duarte, R., Jeffert, J., and Ghosh, D. (1995) *Biochemistry 34*, 6003−6013.
3. Nakajima, K., Hashimoto, T., and Yamada, Y. (1993) *Plant Physiol. 103*, 1465−1466.
4. Hashimoto, T., Nakajima, K., Ongena, G., and Yamada, Y. (1992) *Plant Physiol. 100*, 836−845.
5. Nakajima, K., Yamashita, A., Akama, Y., Nakatsu, T., Kato, H., Hashimoto, T., Oda, J., and Yamada, Y. (1998) *Proc. Natl. Acad. Sci. U.S.A. 95*, 4876−4881.
6. Yamashita, A., Nakajima, K., Kato, H., Hashimoto, T., Yamada, Y., and Oda, J. (1998) *Acta Crystallogr. D54*, 1405−1407.
7. Nickson, A., and Fieser, L. F. (1952) *J. Am. Chem. Soc. 74*, 5566−5570.
8. Otwinowski, Z. (1993) in *Proceedings of the CCP4 Study Weekend* (Sawyer, L., Isaacs, N., and Bailey, S., Eds.) pp 56−62, SERC Daresbury Laboratory, Warrington, England.
9. Collaborative Computational Project, No. 4 (1994) *Acta Crystallogr. D50*, 760−763.
10. Navaza, J. (1994) *Acta Crystallogr. A50*, 157−163.
11. Roussel, A., and Cambillau, C. (1996) *TURBO−FRODO Manual*, AFMB-CNRS, Marseille, France.
12. Brünger, A. T. (1992) *X-PLOR Manual Version 3.1*, Yale University Press, New Haven, CT.
13. Sugio, S., Petsko, G. A., Manning, J. M., Soda, K., and Ringe, D. (1995) *Biochemistry 34*, 9661−9669.
14. Laskowski, R. A., MacArthur, M. W., Moss, D. S., and Thornton, J. M. (1993) *J. Appl. Crystallogr. 26*, 283−291.
15. Ghosh, D., Wawrzak, Z., Weeks, C. M., Duax, W. L., and Erman, M. (1994) *Structure 2*, 629−640.
16. Tanaka, N., Nonaka, T., Tanabe, T., Yoshimoto, T., Tsuru, D., and Mitsui, Y. (1996) *Biochemistry 35*, 7715−7730.

17. Rafferty, J. B., Simon, J. W., Baldock, C., Artymiuk, P. J., Baker, P. J., Stuitje, A. R., Slabas, A. R., and Rice, D. W. (1995) *Structure 3*, 927−938.
18. Tanaka, N., Nonaka, T., Nakanishi, M., Deyashiki, Y., Hara, A., and Mitsui, Y. (1996) *Structure 4*, 33−45.
19. Varughese, K. I., Skinner, M. W., Whiteley, J. M., Matthews, D. A., and Xuong, N. H. (1992) *Proc. Natl. Acad. Sci. U.S.A. 89*, 6080−6084.
20. Andersson, A., Jordan, D., Schneider, G., and Lindqvist, Y. (1996) *Structure 4*, 1161−1170.
21. Su, Y., Varughese, K. I., Xuong, N. H., Bray, T. L., Roche, D. J., and Whiteley, J. M. (1993) *J. Biol. Chem. 268*, 26836−26841.
22. Breton, R., Housset, D., Mazza, C., and Fontecilla-Camps, J. C. (1996) *Structure 4*, 905−915.
23. Schenk, H., MacGillavry, C. H., Skolnik, S., and Laan, J. (1967) *Acta Crystallogr. 23*, 423.
24. Ghosh, D., Pletnev, V. Z., Zhu, D. W., Wawrzak, Z., Duax, W. L., Pangborn, W., Labrie, F., and Lin, S. H. (1995) *Structure 3*, 503−513.
25. Azzi, A., Rehse, P. H., Zhu, D. W., Campbell, R. L., Labrie, F., and Lin, S. X. (1996) *Nat. Struct. Biol. 3*, 665−668.
26. Deslongchamps, P. (1975) *Tetrahedron 31*, 2463.
27. Deslongchamps, P. (1977) *Heterocycles 7*, 1271.
28. Sherrod, M. J., and Menger, F. M. (1989) *J. Am. Chem. Soc. 111*, 2611−2613.
29. Wu, Y. D., and Houk, K. N. (1987) *J. Am. Chem. Soc. 109*, 2226−2227.
30. Wu, Y. D., and Houk, K. N. (1987) *J. Am. Chem. Soc. 109*, 906−908, 908−910.
31. Kraulis, P. J. (1991) *J. Appl. Crystallogr. 24*, 946−950.

BI9825044